

Supporting Information

KAHRP eventually assembles at re-modeled actin junctions and in association with the knob spiral in *P. falciparum*-infected erythrocytes

Cecilia P. Sanchez, Pintu Patra, Shih-Ying Scott Chang, Christos Karathanasis, Lukas Hanebutte, Nicole Kilian, Marek Cyrklaff, Mike Heilemann, Ulrich S. Schwarz*, Mikhail Kudryashev*, and Michael Lanzer*

*corresponding authors: email: michael.lanzer@med.uni-heidelberg.de, schwarz@thphys.uni-heidelberg.de; mikhail.kudryashev@mdc-berlin.de

This PDF file includes

Table S1 and S2

Figure S1 to S14

Supplementary Experimental Procedures

TABLE S1 Antibodies and nanoprobes

Antibodies and nanoprobes	Vendor	Dilutions
mAb Actin, clone AC40 (mouse)	Sigma-Aldrich	1:100
mAb Adducin α , clone 4D1 (mouse)	Santa Cruz Biotechnology	1:100
mAb Tropomodulin 1, OTI2C2 (mouse)	Novus Biologicals	1:100
mAb Spectrin β , B-2 (mouse)	Santa Cruz Biotechnology	1:100
mAb Spectrin β , A-12 (mouse)	Santa Cruz Biotechnology	1:300
Protein 4.1R (rabbit)	Sigma-Aldrich	1:100
Tropomyosin 5NM1, 5NM2 (sheep)	Merck	1:100
mAb Ankyrin-1, H-4 (mouse)	Santa Cruz Biotechnology	1:200
mAb KAHRP, 18.2 (mouse)	The European Malaria Reagent Repository	0.8 μ g/ml
KAHRP ²⁸⁸⁻³⁰² (rabbit)	Costum-made, Eurogentec	1:500
mAb 6xHIS, HIS-H8 (mouse)	Thermo Fisher	1:100
PfEMP1 (ATS) (guinea pig)	Denise Mattei; gift	1:100
MAHRP1 (rabbit)	Hans-Peter Beck; gift	1:200
PF3D7_0532400 (rabbit)	Hans-Peter Beck; gift	1:200
SBP1 (rat)	Catherine Braun-Breton; gift	1:200
Star 580 goat anti-mouse	Abberior	1:200
Star 580 goat anti-guinea pig	Abberior	1:200
Star 580 goat anti-rabbit	Abberior	1:200
Star 580 donkey anti-sheep	Abberior	1:200
Star red goat anti-mouse	Abberior	1:200
Star red goat anti-guinea pig	Abberior	1:200
Star red goat anti-rabbit	Abberior	1:200
Alexa Fluor 647 goat anti-mouse	Thermo Fisher	1:200
Ni ²⁺ -NTA-Atto 647 nanoprobe	Sigma-Aldrich	1:400
Ni ²⁺ NTA 5 nm gold	Nanoprobes	1:30
NTA, Nitrilotriacetic acid		

TABLE S2 Oligonucleotides

Primer name	sequence
KAHRP-5-for	AGA ATA CTC GCG GCC ACT ATG AAA AGT TTT AAG AAC AAA AAT AC
KAHRP-3-rev	TTA CAA AAT GCT TAA CCG CGG TTA ACC ACA GCA TCC TCT TTT CTT C
KAHRP ^{rc} -AflII-for	GGT CCA AAT ATA TTT GCC TTA AGG AAG AGA TTT CC
KAHRP ^{rc} -AleI-rev	TTT TTT CTT TTC ACA GTC GTG GGA CTT ATG TTT TTT G
mEos-1x-AflII-for	GGT CCA AAT ATA TTT GCC TTA AGT GCG ATT AAG CCA GAC
mEos-1x-AflII-rev	TGG AAA TCT CTT CCT TCG TCT GGC ATT GTC AGG C
KAHRP-guide3-for	TAA GTA TAT AAT ATT TA TAG CGG CAG GTC CAC ATG GTT TTA GAG CTA GAA
KAHRP-guide3-rev	TTC TAG CTC TAA AAC CAT GTG GAC CTG CCG CTA TA AAT ATT ATA TAC TTA
KAHRP-guide4-for	TAA GTA TAT AAT ATT CAT GAA GGA AAT GAC GGT GA GTT TTA GAG CTA GAA
KAHRP-guide4-rev	TTC TAG CTC TAA AAC TCA CCG TCA TTT CCT TCA TG AAT ATT ATA TAC TTA
P1	GTT TAT TTG AAC AAT ATT TAC TCC
P2	ACC ACA GCA TCC TCT TTT CT

Red indicates sequences used for In Fusion-based cloning

Re-codonized KAHRP fragment between the AflII and AleI endo restriction sites

GCTTGAGGAAGAGATTCCATTGGGTATGAACGACGAAGATGAAGAAGGTAAA
 GAAGCTTGGCCATCAAAGATAAGTTGCCAGGTGGTTGGATGAATAACCAAAATC
 AGTTGTACGGTATCTGTAACGAAACTTGTACTACTTGTGGTCCAGCTGCTATTGAT
 TATGTTCCAGCTGATGCTCCAAATGGTTATGCTTATGGTGGTTCTGCTCATGATGG
 TTCACATGGTAATTGAGAGGTCATGGTAACAAAGGTTCTGAAGGTTATGGTTAT
 GAAGCTCCATACAATCCAGGTTTAATGGTGCTCCAGGTTCAAATGGTATGCAAA
 ATTACGTTCCACCACATGGTGGTTATTCTGCTCCATATGGTGGTCCATGGT
 GCAGCTCATGGTTCTAGATATTCTCATTCTCCGTCAACAAATACGGTAAACA
 TGGTGACAAAAGCACCCTTCTAAGAACATGAAGGTAATGATGGTGAGGGT
 GAAAAGAAGAAGAAGTCCAAAAACACAAGGATCACGATGGCGAGAAAAAGAA
 GAGTAAAAAGCACAAAGATAACGAGGATGCCAATCCGTTAAGAGCAAAAACA
 TAAGTCCCACGAC

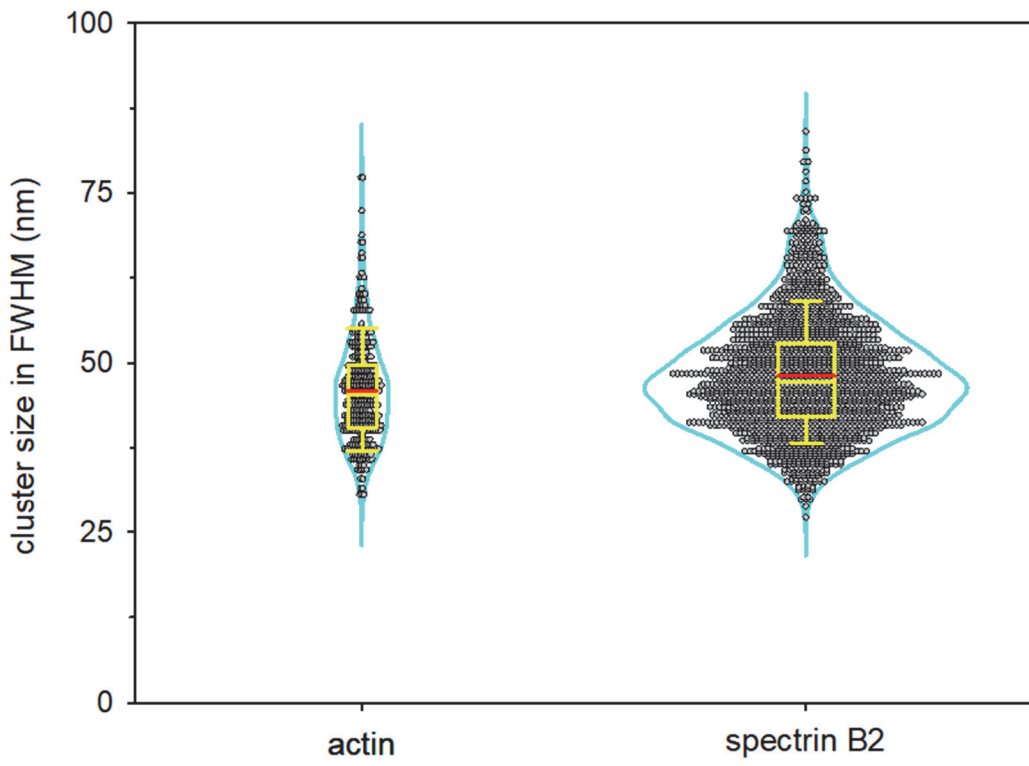


FIGURE S1 Cluster sizes in FWHM of actin and β -spectrin N-terminus (spectrin B2) of uninfected erythrocytes. Violin plots consisting of the Kernel density (cyan), the original data points and a box plot analysis. The box plots show the median (yellow horizontal line), the mean (red horizontal line) and the 25% and 75% quartile ranges. Error bars indicate the 10th and 90th percentile. Actin: N=357, n=23; N-terminus of β -spectrin: N=2220, n=61.

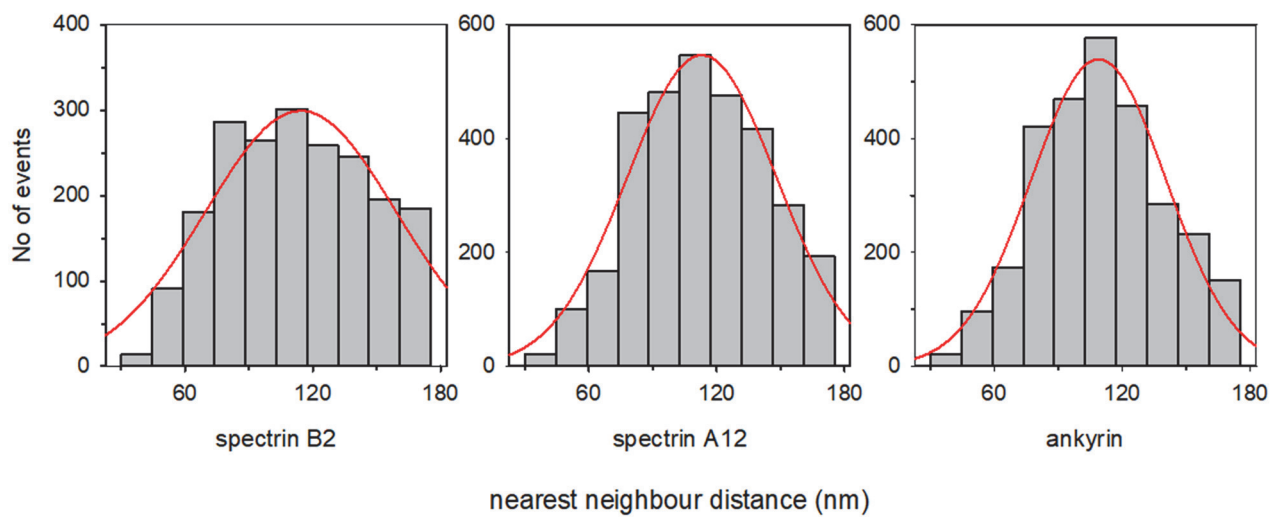


FIGURE S2 Histograms showing the nearest neighbor distance of β -spectrin N-terminus (spectrin B2), β -spectrin C-terminus (spectrin A12) and ankyrin. A Gaussian function was fit to the data (red line).

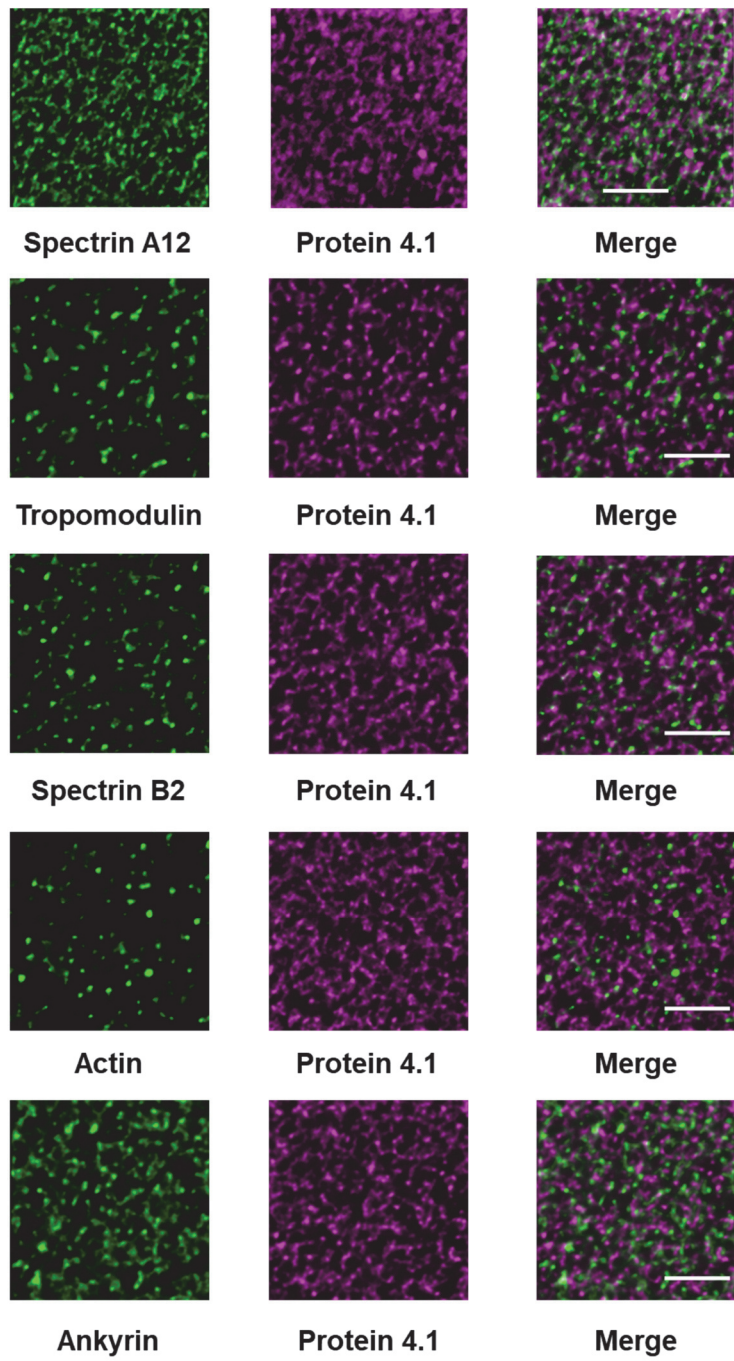


FIGURE S3 Representative STED images of exposed membrane skeletons from uninfected erythrocytes stained with antibodies to the targets indicated. The two channels and the overlay are shown. Scale bar, 1 μ m.

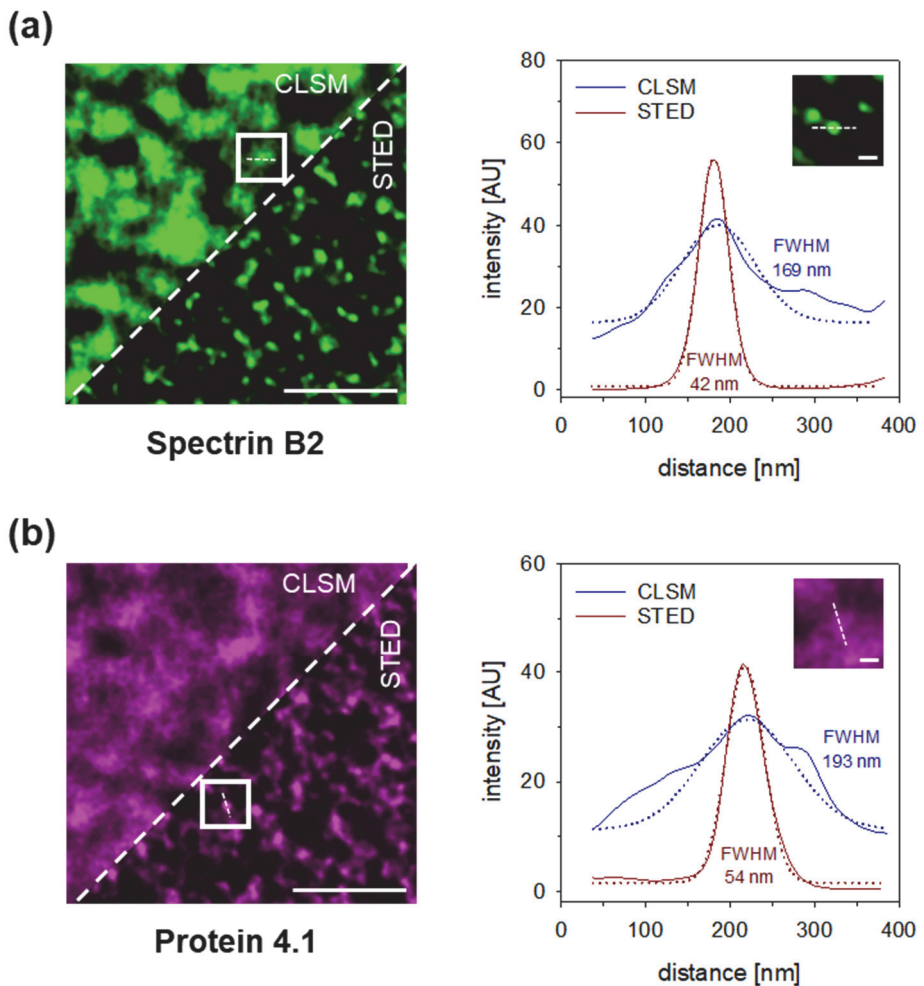
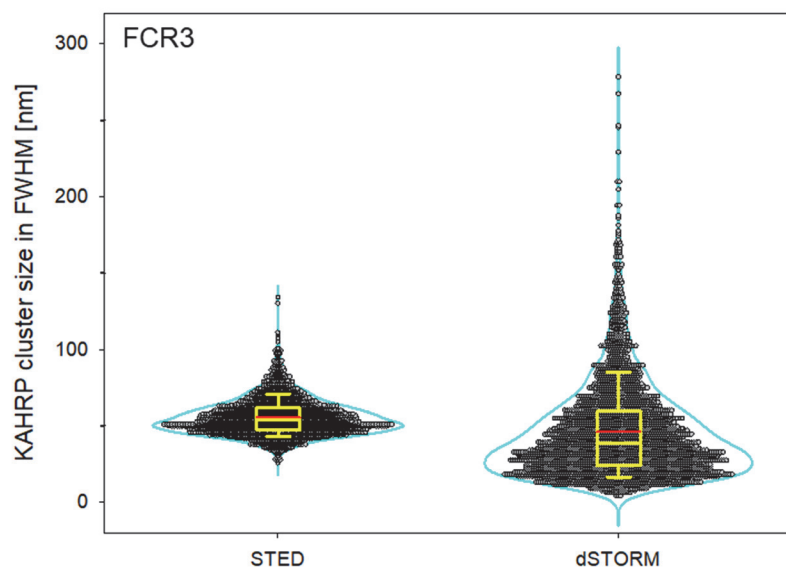


FIGURE S4 Comparison of confocal laser scanning microscopy (CLSM) and STED images of exposed membranes prepared from uninfected erythrocytes and stained with antibodies against the N-terminus of β -spectrin (spectrin B2) and protein 4.1R. (a) Split image showing confocal laser scanning microscopy (CLSM) and STED image. The following antisera were used: mouse monoclonal antibody spectrin B2 and goat anti-mouse antibody conjugated with Abberior star 580. Scale bar, 1 μ m. White box and dashed line indicate the position of line profiles shown on the right. Gaussian fits to the intensity profiles (solid lines) are shown as dashed lines. Inset shows the STED image corresponding to the boxed area. Scale bar, 50 nm. (b) As in A., using a rabbit anti-protein 4.1R antiserum and an Abberior star red conjugated goat anti rabbit antiserum. The inset show the CLSM image corresponding to the boxed area.

(a)



(b)

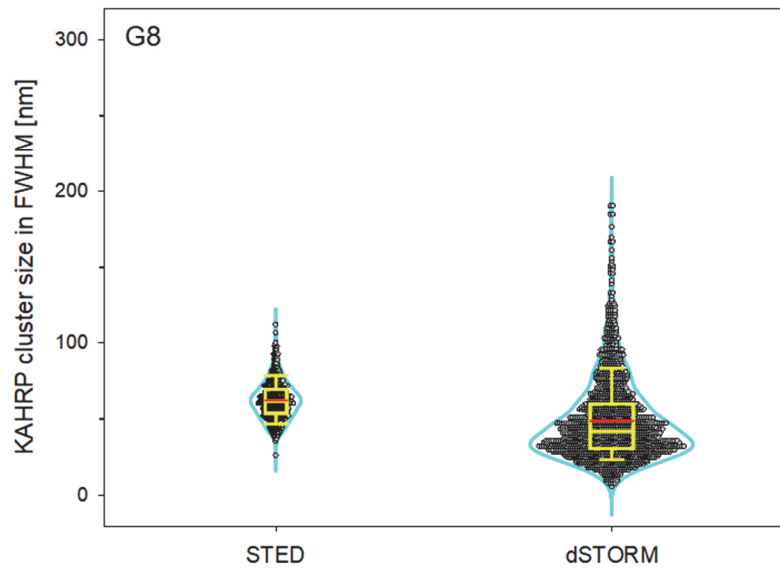


FIGURE S5 KAHRP cluster sizes in FWHM of the parental line FCR3 (a) and the KAHRP/mEOS-expressing mutant G8 (b), as determined by STED and dSTORM microscopy. Violin plots consisting of the Kernel density (cyan), the original data points and a box plot analysis. The box plots show the median (yellow horizontal line), the mean (red horizontal line) and the 25% and 75% quartile ranges. Error bars indicate the 10th and 90th percentile. FCR3: N=2800, n=267 for STED and N=3383, n=14 for dSTORM. G8: N=646, n=29 for STED and N=1708, n=30 for dSTORM.

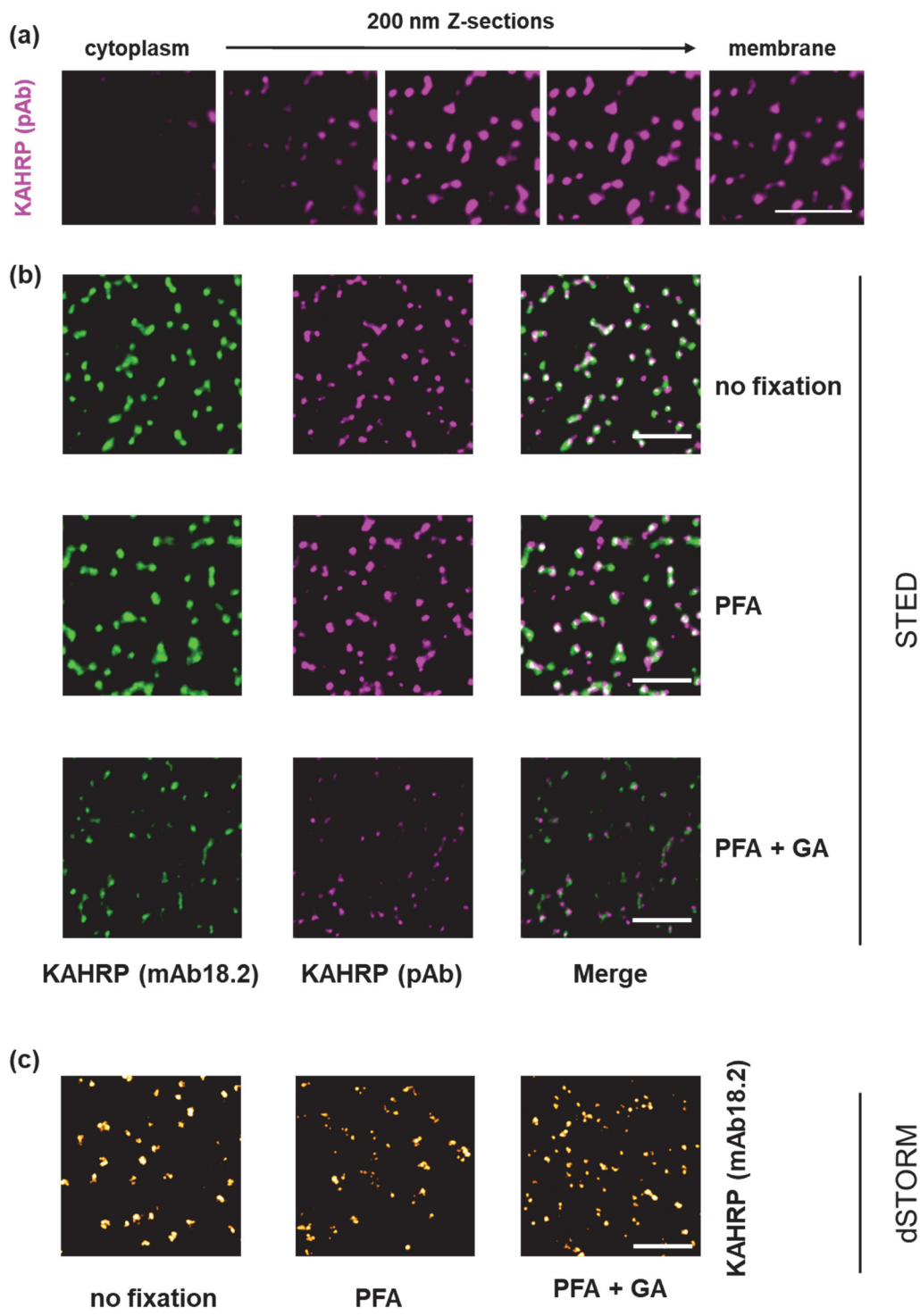
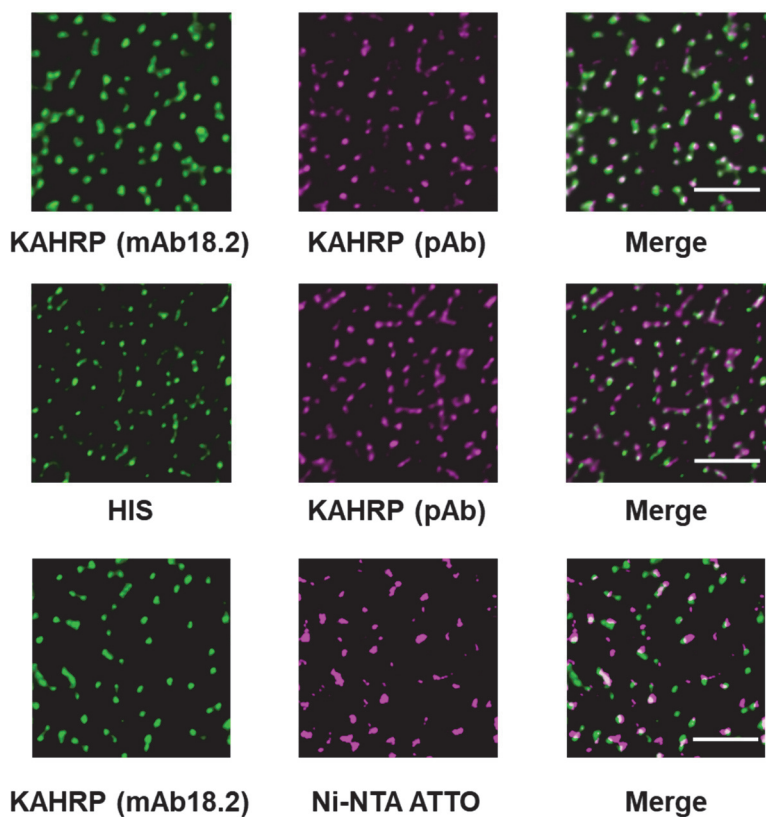


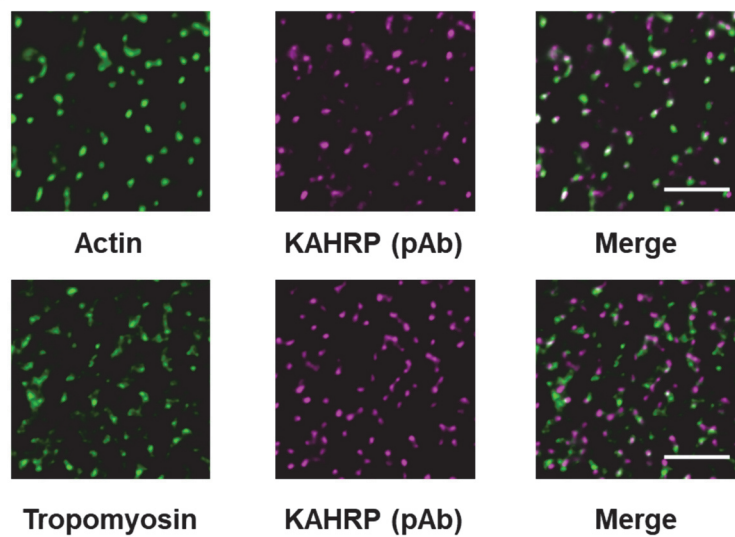
FIGURE S6 Super-resolution imaging of KAHRP under different fixation conditions. (a) 3D STED imaging of exposed trophozoite membranes, using the anti-KAHRP peptide antiserum. 200 nm z-sections are shown. Scale bar, 0.5 μ m. (b) Exposed trophozoites membranes were unfixed, fixed with 4% paraformaldehyde (PFA), or fixed with 4% paraformaldehyde and 0.0065% glutaraldehyde (PFA + GA) for 15 min before the sample was stained with the

monoclonal anti KAHRP antibody mAB18.2 and the anti-KAHRP peptide antiserum. Representative STED images are shown. Scale bar, 1 mm. (c) Representative dSTORM images of unfixed and fixed anti-KAHRP stained (mAB18.2) exposed membranes from trophozoites. Scale bar, 1 μ m.

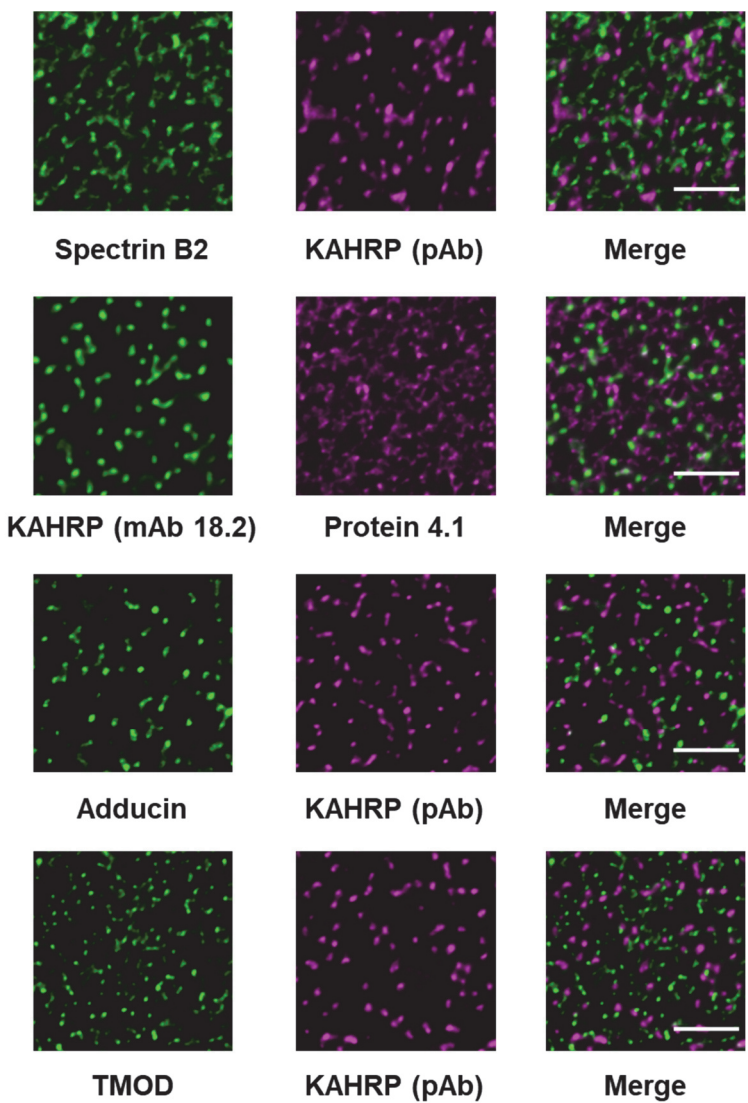
(a)



(b)



(c)



(d)

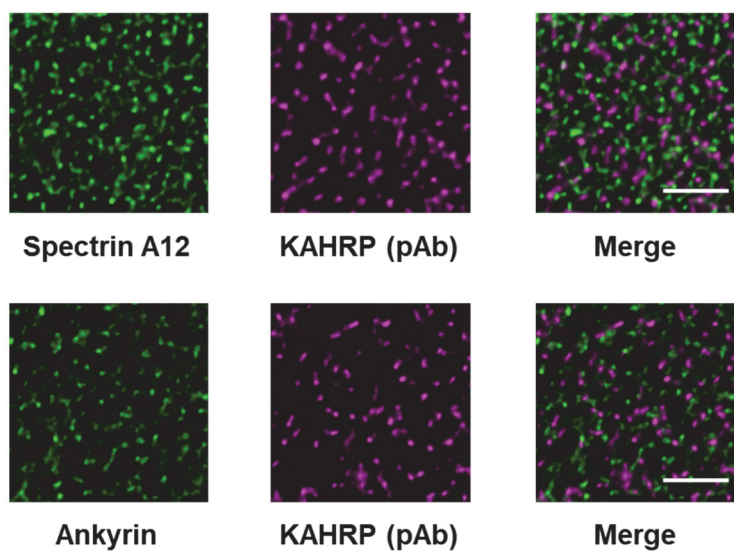
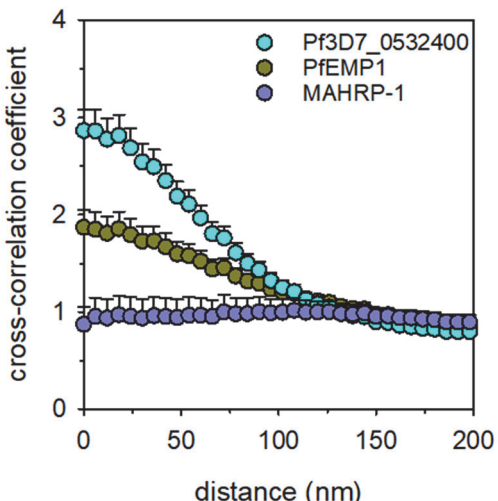


FIGURE S7 Two-color STED images of exposed membranes prepared from trophozoites, showing KAHRP and a component of the membrane skeleton. Separate STED images of the two channels and an overlaid STED image are shown. Scale bar, 1 μ m. (a) Various probes targeting KAHRP, including the monoclonal antibody mAB18.2, the peptide antiserum pAB, a monoclonal anti-histidine antibody (His), and a Ni²⁺-NTA-ATTO nanoprobe. (b) Targeting KAHRP using the peptide antiserum pAB and actin and tropomyosin, two components of the actin junctional complex. (c) Targeting KAHRP using the antiserum indicated and components of the actin junctional complex, including the N-terminus of β -spectrin (spectrin B2), protein 4.1R, adding and tropomodulin (TMOD). (d) Targeting KAHRP and the C-terminus of β -spectrin (spectrin A12) and ankyrin, two components of the ankyrin bridge.



(b)

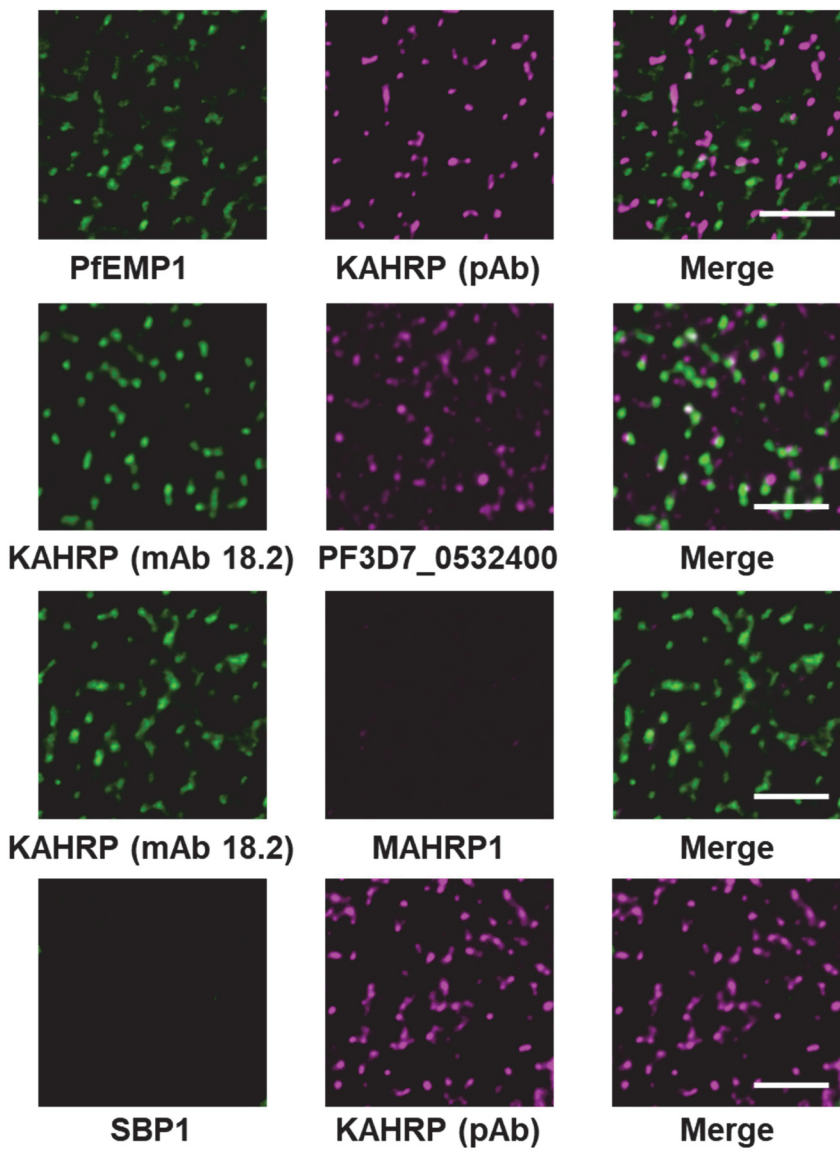
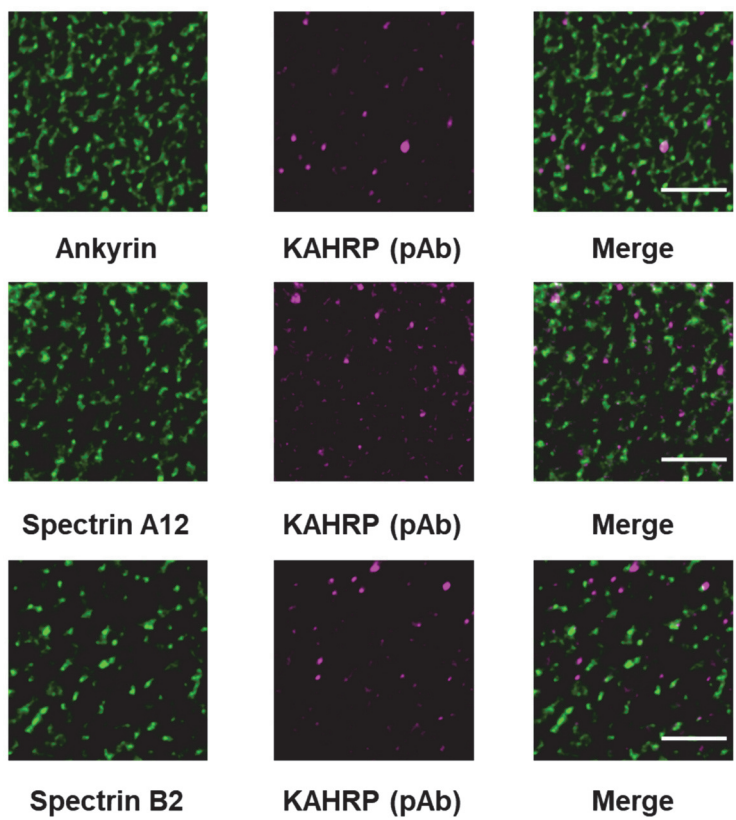
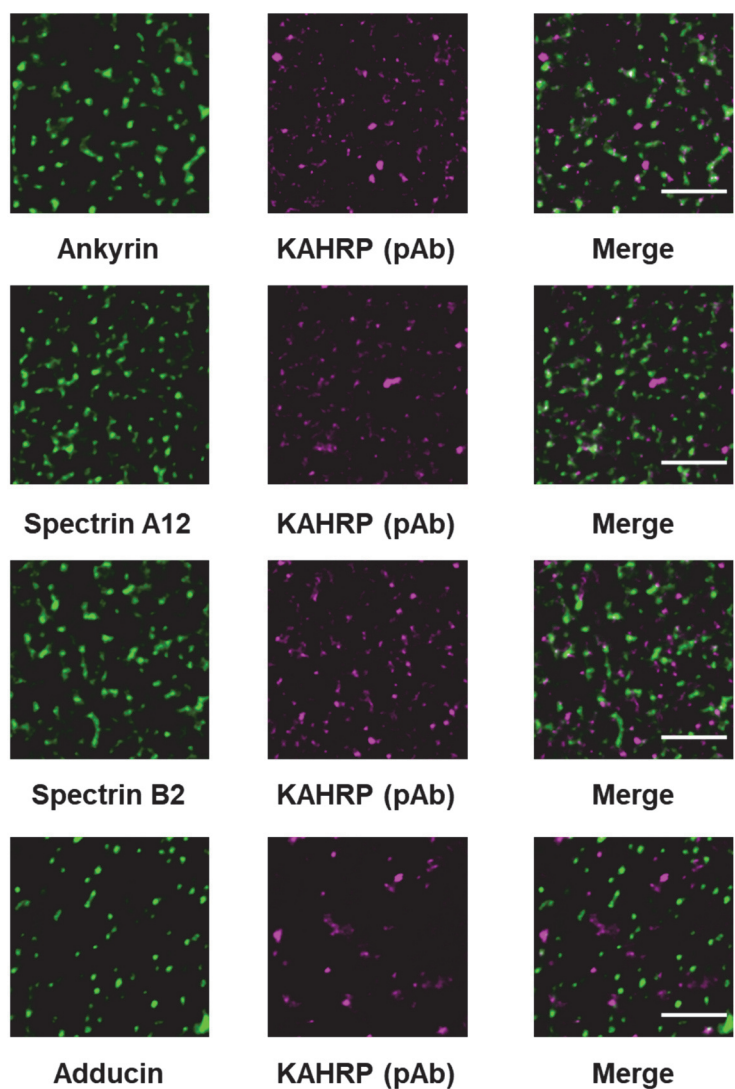


FIGURE S8 Co-localization of KAHRP with PfEMP1 and PHIS1605w and not MAHRP1. (a) Calculated two-dimensional cross-correlations between KAHRP (using pAB) and PHIS1605w (cyan; n=26), PfEMP1 (olive green; n=15) and MAHRP1 (violet; n=14). The means \pm SEM of n cells from at least three different donors are shown. (b) Two-color STED images of exposed membrane skeletons from trophozoite labeled with antisera against KAHRP, PfEMP1, PHIS1605w; MAHRP1, and SBP1. Separate STED images of the two channels and an overlaid STED image are shown. Scale bar, 1 μ m

(a)



(b)



(c)

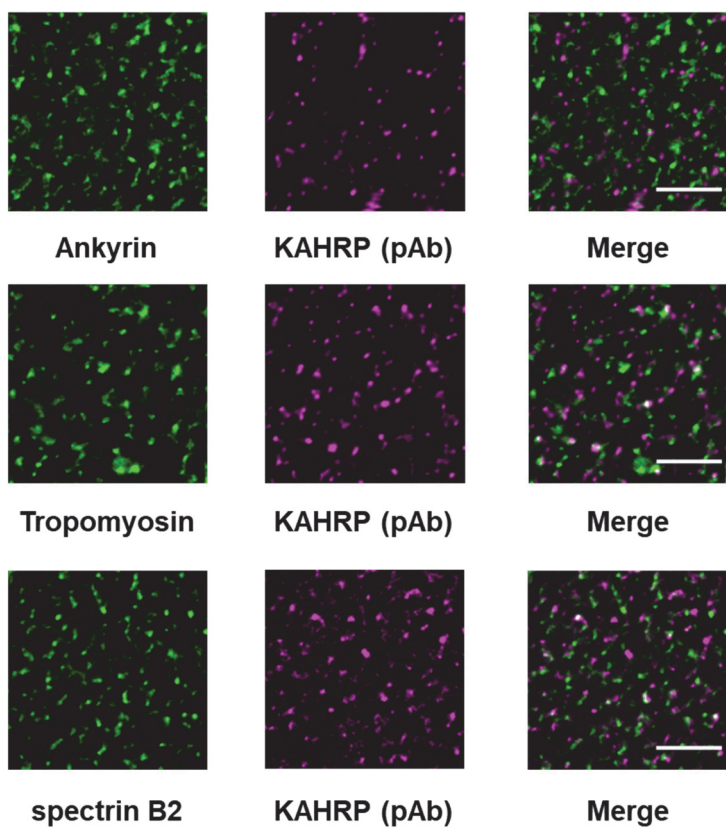


FIGURE S9 Two-color STED results of exposed membranes prepared from highly synchronized parasite cultures. Separate STED images of the two channels and an overlaid STED image are shown. Scale bar, 1 μ m. (a) Exposed membranes were prepared from highly synchronized parasite cultures 12 \pm 2 hours post invasion and stained with antisera against KAHRP, ankyrin, N-terminus β -spectrin (spectrin B2) and C-terminus of β -spectrin (spectrin A12). (b) as in A but investigating parasites 16 \pm 2 hours post invasion. (c) as in A but investigating parasites 20 \pm 2 hours post invasion

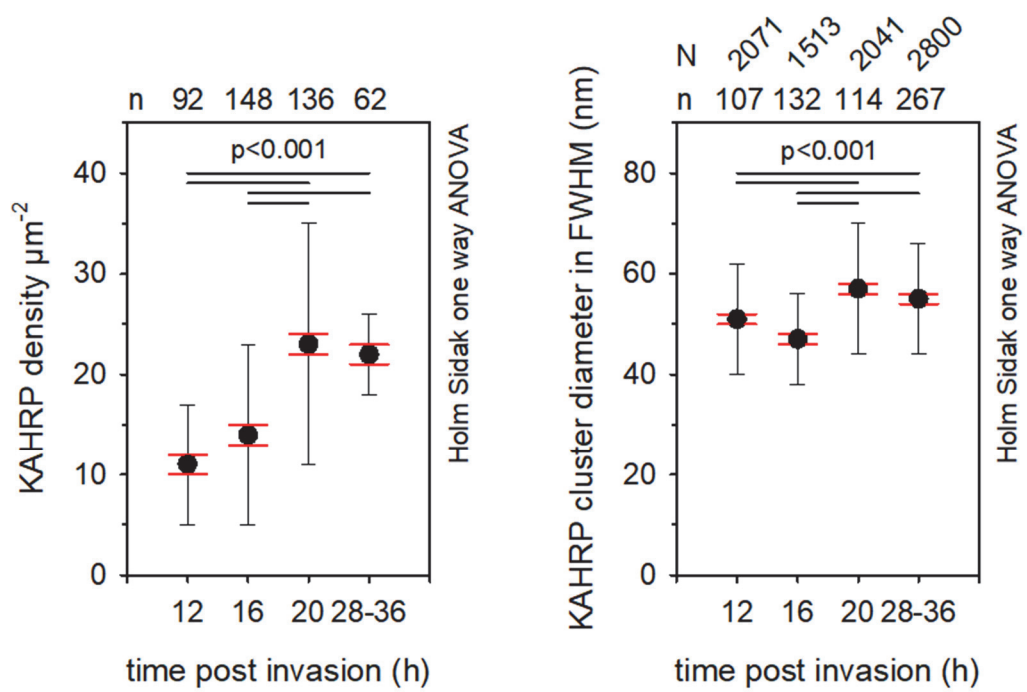


FIGURE S10 KAHRP signal density and size in FWHM as a function of time post invasion. The means \pm SEM of N determinations from n cells are shown. Values for N and n are provided above the respective graphs. Statistical significance was assessed using the Holm Sidak one way ANOVA test.

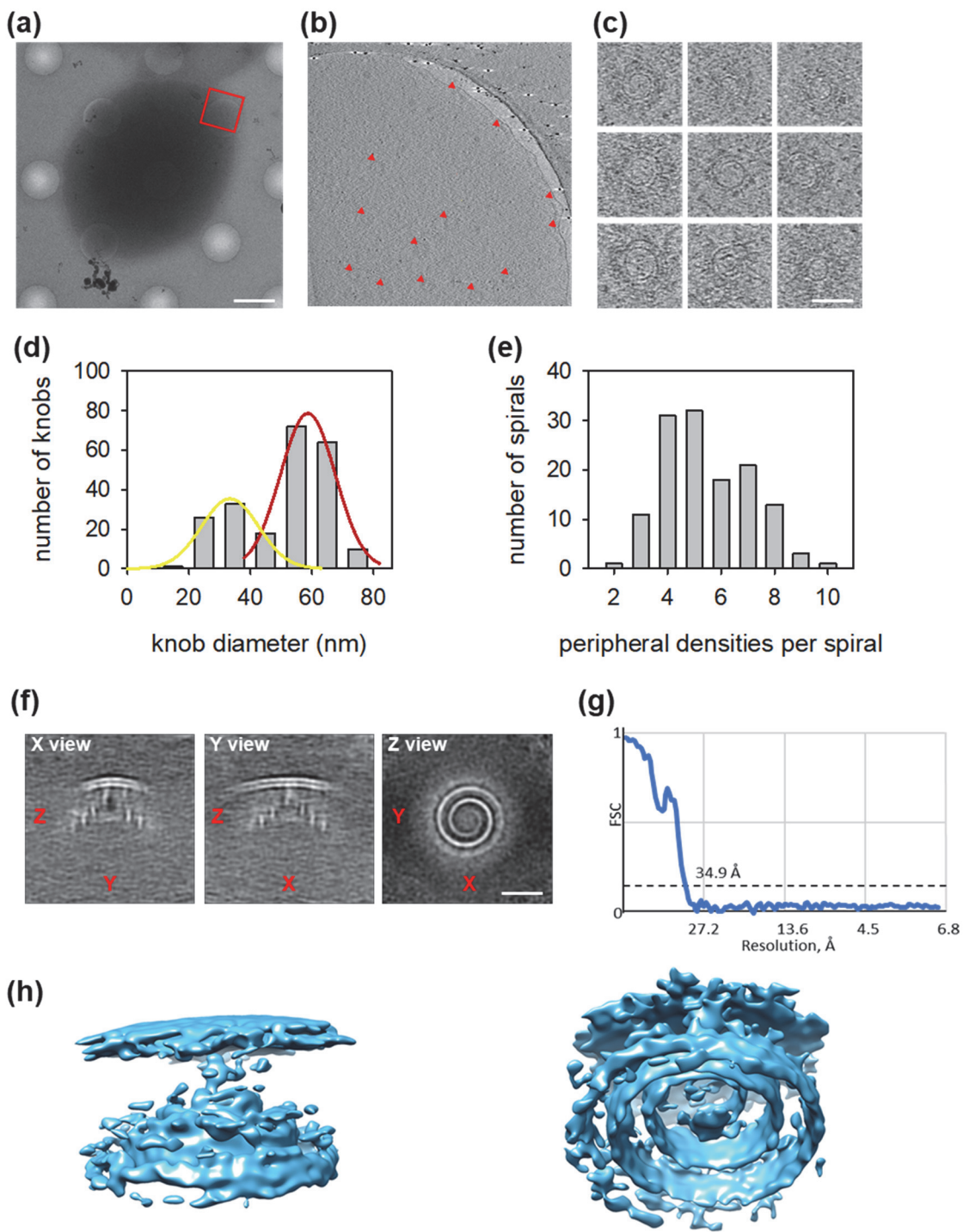


FIGURE S11 Cryo-tomography of knob spiral. (a) Low magnification cryo-image of a membrane ghost prepared from a trophozoite infected erythrocyte. The image shows the ghost deposited on a holey EM-grid (Quantifoil 2/1). The red box indicates an area highlighted in (B). Scale bar: 2 μm. (b) An area for automated data acquisition is shown. Knobs and knob spirals in top views and side views are marked by red triangles. Scale bar, 200 nm. (c) Examples of top and side views of knobs.

views of spirals. Scale bar, 50 nm. (d) Measurements of the radius for individual knobs. (e) Number of peripheral crown-like densities per spiral. (f) Subtomogram averages filtered to 35 Å resolution without and with the applied mask used for processing (see Figure S14). (g) A Fourier shell correlation indicated a resolution of the reconstruction of 35 Å. (h) volume-rendered representation of the spiral and associated plasma membrane. Side and skew views of the knob spiral are shown.

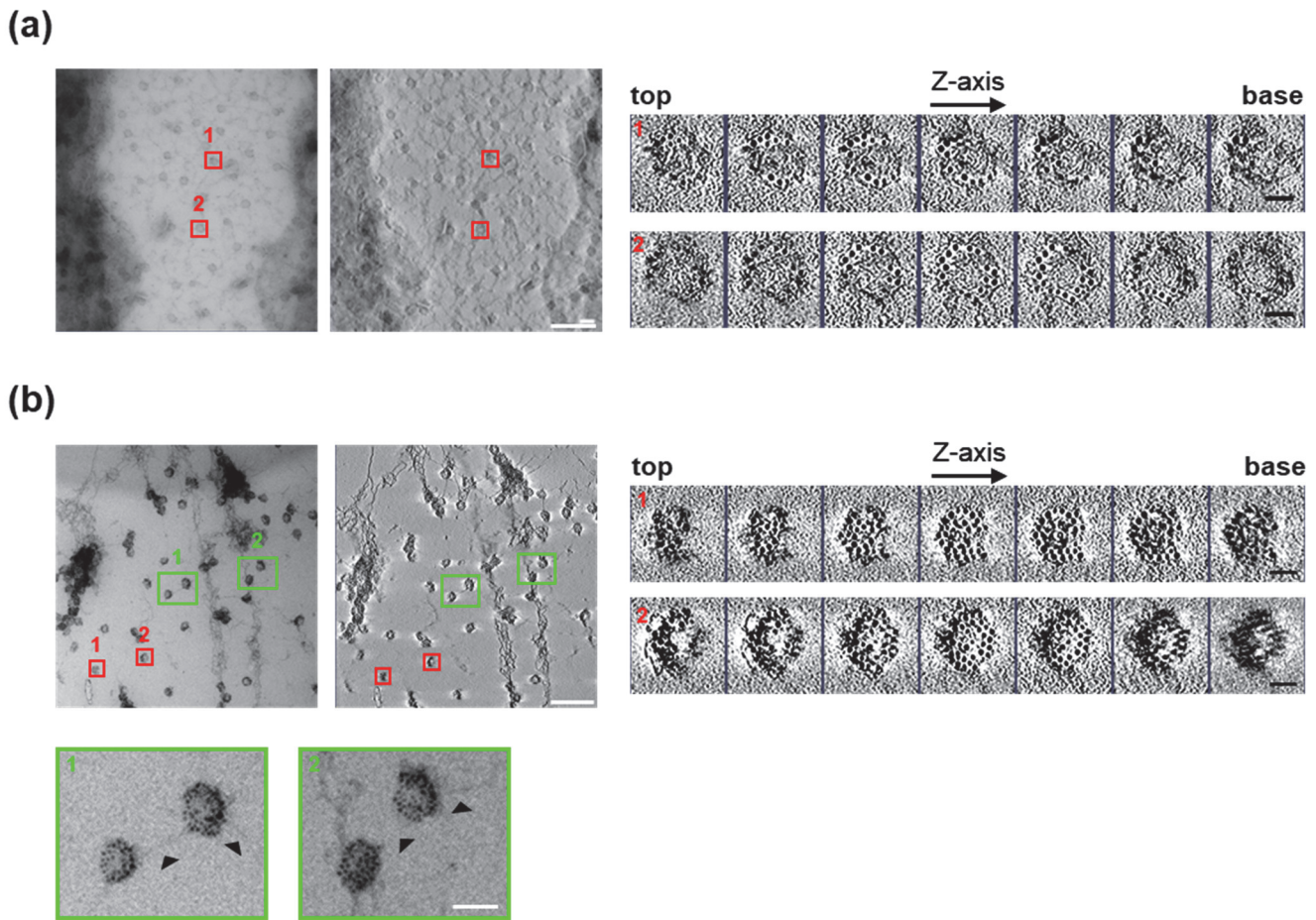


FIGURE S12 Immuno-EM labeling of the knob spiral with a Ni^{2+} -NTA 5 nm gold nanoprobe.

(a) Methyl cellulose embedded trophozoite membrane ghosts extracted with 0.2% NP40 Substitution and labelled with the Ni^{2+} -NTA 5 nm gold nanoprobe. Left: Transmission electron microscopic image (left image) and the corresponding tomographic reconstruction. Right: consecutive z-sections from an EM-tomogram showing labeling of the knob spiral scaffold with the Ni^{2+} -NTA 5 nm gold nanoprobe. The boxes indicate representative extracted volumes that were subsequently displayed in z-sections. The sections are shown from left to right from the top of the spiral to the base. Scale bars, 1 μm main images and 30 nm sub-images. (b) As in A, but analyzing trophozoite membrane ghost extracted with 1% NP40 Substitution. Green boxes: zoomed-in areas highlighting filaments extending from the spiral scaffold indicated by arrowheads). Scale bar, 100 nm

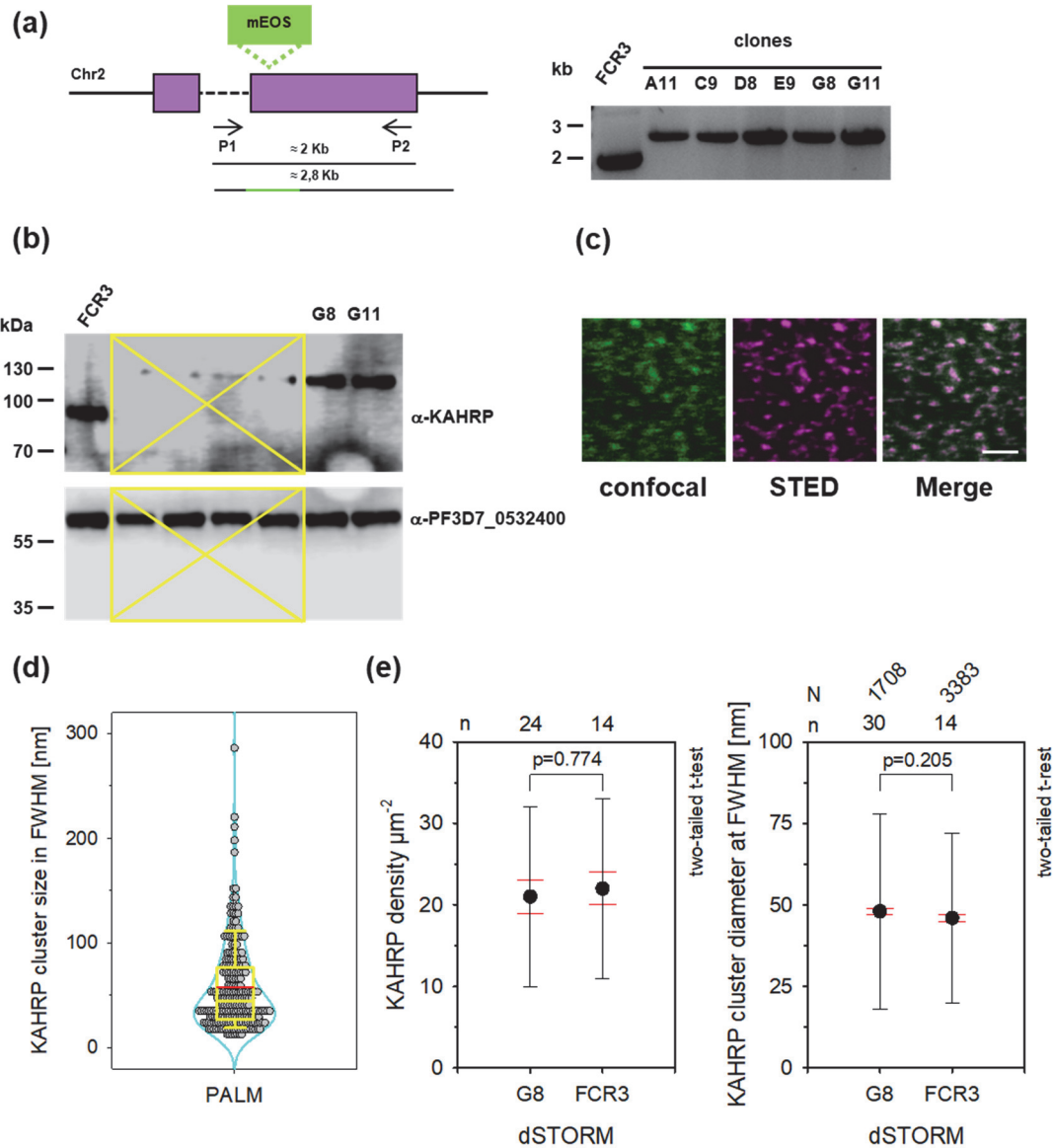
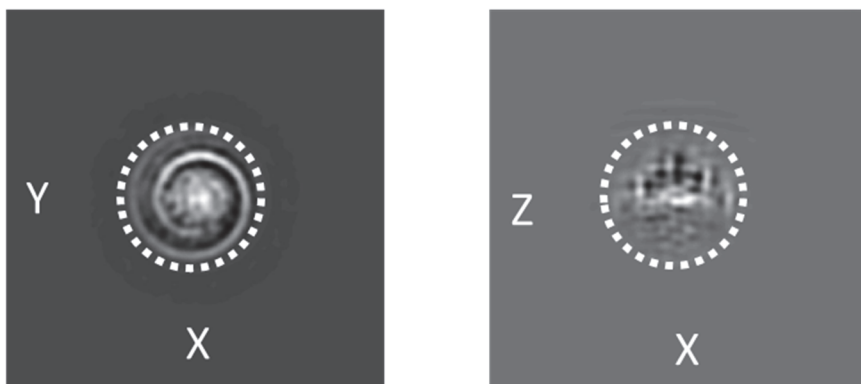


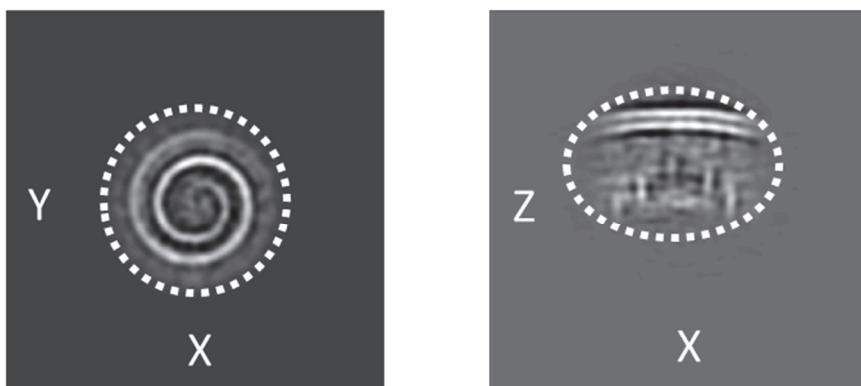
FIGURE S13 Generation and analysis of a KAHRP/mEOS2 expressing *P. falciparum* mutant line. (a) Genomic organization of the *kahrp* locus on chromosome 2. The coding sequence of mEOS2 is indicated, as is the integration site. Relevant primers used for analysis of genetically altered lines and corresponding fragment lengths are shown. The phaerogram shows the result of a PCR analysis of genomic DNA prepared from the parental line FCR3 and five clonal mutant lines, using primers P1 and P2. The PCR products were sequenced and the insertion of the mEOS2 coding sequence in the *kahrp* coding sequence was confirmed in all mutant lines. A size marker is indicated in kb. (b) Western analysis using the anti-KAHRP peptide antibody (pAB).

Note the shift in KAHRP signal in the investigated mutant lines G8 and G11, as compared with the parental line FCR3. An anti-serum to PFE1605w was used as a loading control. A size marker is indicated in kDa. (c) Imaging an exposed membrane prepared from the KAHRP/mEOS2 mutant G8 by correlative confocal fluorescence microscopy (left image; excitation wavelength, 488 nm and emission wavelength, 500-550 nm bandpass filter) and STED microscopy (STED) using the anti-KAHRP monoclonal mouse antibody mAB18.2 and an anti-mouse starred conjugated antibody (excitation wavelength, 640 nm and emission wavelength, 685-670 nm bandpass filter). The overlay of both images is shown. Scale bar, 1 μ m. (d) KAHRP cluster size in FWHM of the KAHRP/mEOS-expressing mutant G8 (B), as determined by PALM. Kernal density pots with the original data points are shown. The box plots show the median (yellow horizontal line), the mean (red horizontal line) and the 25% and 75% quartile ranges. N=237, n=15. (e) Comparison of KAHRP cluster size in FWHM and distribution density from G8 and the parental line FCR3, as determined using dSTORM. Statistical significance was assessed using two-tailed t-test.

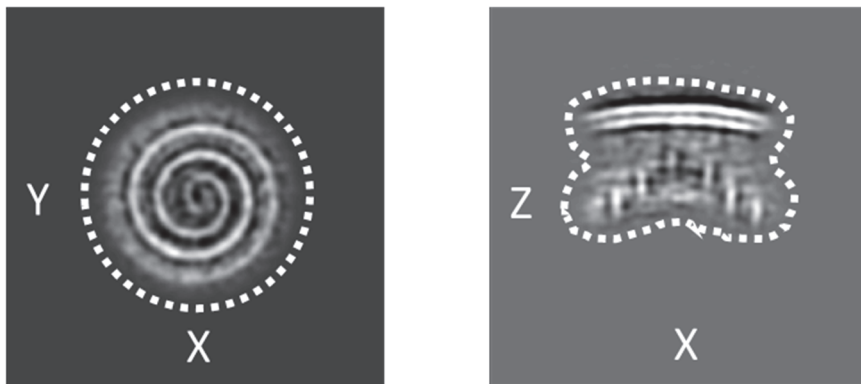
(a)



(b)



(c)



top view

side view

FIGURE S14 Masks used for analysis of spirals. (a) A small sphere mask was applied to the core region of spirals for initial structural analysis. (b) A larger ellipsoid mask covering the whole knob was used for classification. (c) A dumbbell-like mask was used for the refinement and FSC determination. x,y,z directions are indicated.

**Supplementary Materials for
KAHRP dynamically relocates to remodeled actin junctions and associates
with knob spirals in *P. falciparum*-infected erythrocytes**

Cecilia P. Sanchez, Pintu Patra, Shih-Ying Scott Chang, Christos Karathanasis, Lukas Hanebutte, Nicole Kilian, Marek Cyrklaff, Mike Heilemann, Ulrich S. Schwarz*, Mikhail Kudryashev, and Michael Lanzer*

Pair cross-correlation between two image channels

To compute cross-correlation between a pair of images, we follow the following step. First, we define two dimensional pair distance distribution (PDD) $P(r)$ for two images ($I_R(x, y)$, red channel and $I_G(x, y)$, green channel) [1, 4] as

$$P(r) = \frac{\sum_{i,j} \sum_{m,n} I_R(x_i, y_j) I_G(x_m, y_n) \delta(|\mathbf{r}_{ij} - \mathbf{r}_{mn}| - r)}{\sum_{i,j} \sum_{m,n} I_R(x_i, y_j) I_G(x_m, y_n)}. \quad (1)$$

A histogram of pair distance distribution is computed by using bins of width Δr as

$$P(r, r + \Delta r) = \sum_{\rho=r}^{\rho=r+\Delta r} P(\rho). \quad (2)$$

Next, we radially average the resultant distribution to account for the increase in the area of radial bins. Specifically, we use fractional area, i.e., the area of each bin with respect to the image area, as the normalization factor $N(r)$ [4, 6], which is given by

$$N(r) = \frac{\pi \Delta r (2r + \Delta r)}{A_{image}}. \quad (3)$$

The normalization factor makes the distribution dimensionless and analogous to the cross-correlation function defined for localization points [3, 6]. The resultant distribution is the cross-correlation distribution (PCC) for two images,

$$C(r, r + \Delta r) = \frac{A_{image}}{\pi \Delta r (2r + \Delta r)} \sum_{\rho=r}^{\rho=r+\Delta r} \frac{\sum_{i,j} \sum_{m,n} I_R(x_i, y_j) I_G(x_m, y_n) \delta(|\mathbf{r}_{ij} - \mathbf{r}_{mn}| - \rho)}{\sum_{i,j} \sum_{m,n} I_R(x_i, y_j) I_G(x_m, y_n)}. \quad (4)$$

The above expression can be reduced for localization points data by using $I_R = \sum_{k=1}^{n_R} \delta(\mathbf{r}_i - \mathbf{r})$, the localisation points in red and $I_G = \sum_{k=1}^{n_G} \delta(\mathbf{r}_j - \mathbf{r})$, the localisation points in green. This leads to the expression PCC as

$$C(r, r + \Delta r) = \frac{\sum_{\rho=r}^{\rho=r+\Delta r} \sum_{i=1}^{n_R} \sum_{j=1}^{n_G} \delta(|\mathbf{r}_i - \mathbf{r}_j| - \rho)}{\pi \Delta r (2r + \Delta r) \eta}, \quad \eta = \frac{n_R \times n_G}{A_{image}} \quad (5)$$

The numerator is evaluated by making a histogram of pairwise distances of single-molecule localization points from two images. The denominator is calculated by repeating the same procedure with an equal number of randomly distributed points of two colors in the same area. The average distance distribution for randomly distributed data-set is given by $\pi \Delta r (2r + \Delta r) \eta$, where η is the density of pair-wise distances [4, 6]. This method has been used in the recent works [3–6] for super-resolution microscopy localization data-sets.

Image re-sampling helps to improve cross-correlations at short distances.

The first step for estimating cross-correlation is the numerical calculation of pair distance distribution (PDD) from images. We notice PDD at short distances is limited by the pixel dimension of the image, e.g., the minimum separation distance can be 1 pixel. To estimate PDD at short distances, we interpolate the images to finer pixels using image re-sampling. This procedure does not lose any information as a single fluorescence signal covers multiple pixels. Specifically, we divide each pixel area into smaller grids (Fig. 1a)

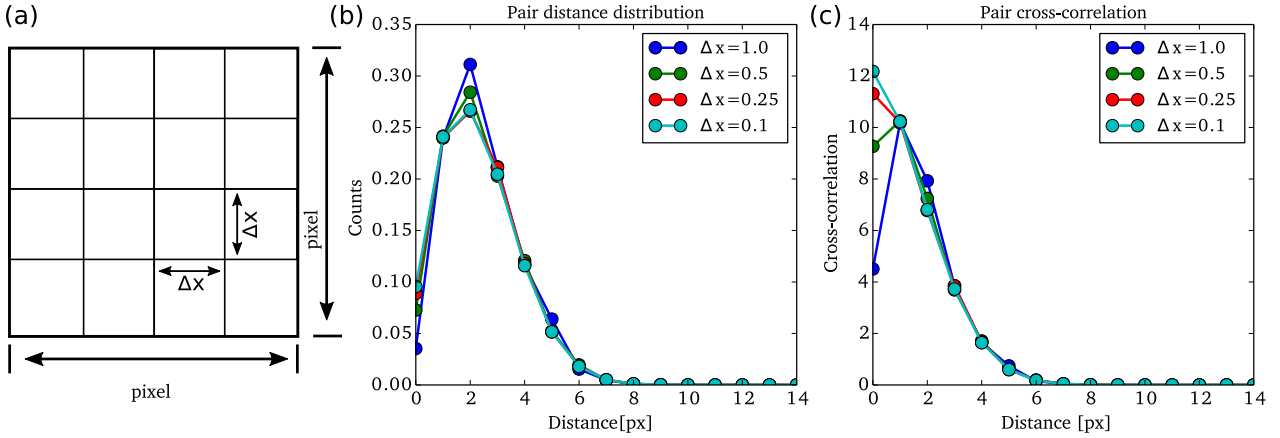


FIG. 1: (a) Each image pixel in the original image is subdivided into multiple smaller pixels with an area $\Delta x \Delta x$. (b) Normalised pair-distance distribution for two 2D-gaussian separated by a distance of 0 pixel. (c) Pair cross-correlation function for two 2D-gaussian separated by a distance 0 px for different Δx values.

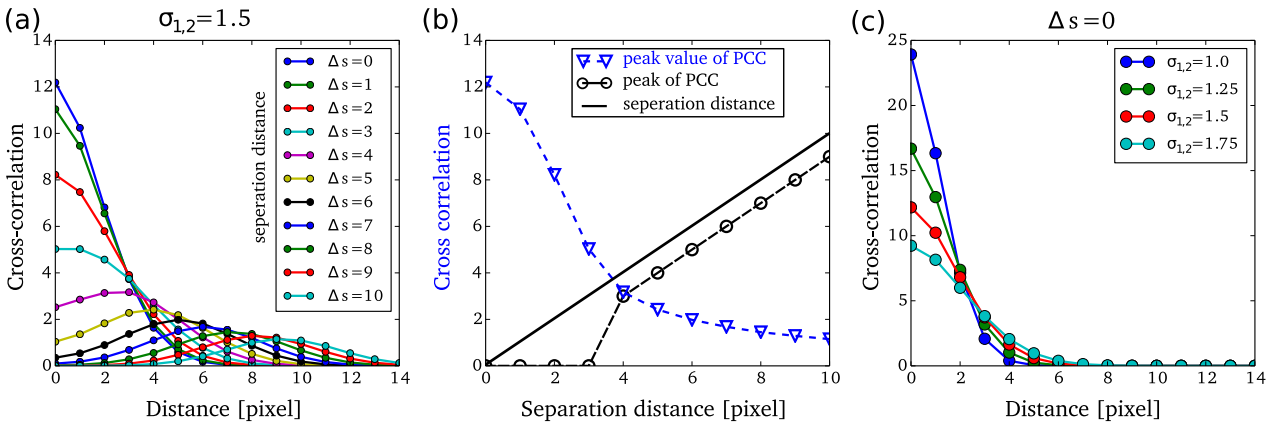


FIG. 2: (a) Pair cross-correlation distribution for different separation distances (Δs) of the signal pairs. (b) Separation estimated from the peak distance value in PCC and corresponding PCC value. (c) Pair cross-correlation distribution for different standard deviation of the two signals for zero separation.

and interpolate the signal intensity using bi-linear interpolation. The improvement from this step saturates as the grid size becomes smaller, as shown in Fig. 1b. We choose $\Delta x = 0.1$ pixel for all the experimental images. The cross-correlation distribution also improves due to the improvement in PDD. The peak in cross-correlation shifts to zero from a one-pixel distance (Fig 1c).

The pair cross-correlation function is highest at zero inter-molecular distance for smaller separation (particularly when the separation distance d is comparable to $\sqrt{\sigma_1^2 + \sigma_2^2}$, where $\sigma_{1,2}$ are the standard deviations for the two signals [1, 2]). The cross-correlation value at zero distance increases as the inter-molecular distance decreases (Fig. 2a). At the large separation distances, the pair correlation function shows a peak at finite distance (Fig. 2b).

Another factor that influences the cross-correlation value is the noise in fluorescence signals. Increase in the standard deviation in signals decreases cross-correlation value (Fig. 2c). Physically, this means sharper signals will lead to higher cross-correlation values compared to broader signals for a fixed separation distance. For our analysis, we choose a binwidth $\Delta r = 0.4$ pixel = 6 nm (1 pixel = 15 nm). The code for cross-correlation analysis is written in Python.

Python code for computation of pair cross-correlation

```

1 import numpy as np
2 import matplotlib.pyplot as plt
3 from scipy import interpolate
4 from scipy.spatial.distance import cdist
5 from PIL import Image
6
7 ROIval=np.loadtxt('ROI.txt')#Input file for region of interest
8 Xmin = int(ROIval[0])
9 Ymin = int(ROIval[1])
10 Xmax = int(ROIval[2])
11 Ymax = int(ROIval[3])
12
13 filename1='STARRED'
14 filename2='594'
15 threshold=20 #Intensity below this value is considered as noise
16
17 img1 = Image.open(str(filename1)+'.tif') #Loading image 1
18 image1 = np.array(img1) #Converting image in array
19 image1 = image1[0:,0:,0] #Selecting the right channel (RGB) of the image array: 0 for red
20 image1[image1<=threshold]=0 #Image thresholding
21 image1=image1[Ymin:Ymax,Xmin:Xmax] #Interested region is cropped out
22
23 #Same steps are repeated for Image 2
24 img2 = Image.open(str(filename2)+'.tif')
25 image2 = np.array(img2)
26 image2 = image2[0:,0:,1] #Selecting the right channel (RGB) of the image array: 1 for green
27 image2[image2<=threshold]=0
28 image2=image2[Ymin:Ymax,Xmin:Xmax]
29
30 #Image resampling or interpolation
31 x = np.arange(0, Xmax-Xmin, 1) #Existing x-grid
32 y = np.arange(0, Ymax-Ymin, 1) #Existing y-grid
33 f1 = interpolate.interp2d(x, y, image1, kind='linear')
34 f2 = interpolate.interp2d(x, y, image2, kind='linear')
35
36 dxy=0.1 #New grid spacing
37
38 xnew = np.arange(0, Xmax-Xmin, dxy) # New x-grid
39 ynew = np.arange(0, Ymax-Ymin, dxy) # New y-grid
40 image1 = f1(xnew, ynew) #Resampled image 1
41 image2 = f2(xnew, ynew) #Resampled image 2
42
43 image1new=image1.copy()
44 image2new=image2.copy()
45
46 loc1=np.array(np.where(image1new!=0)).T #Contains coordinates of the non-zero grids
47 val1=image1[np.where(image1new!=0)]*1.0 #Contains intensity values of such grids.
48 loc2=np.array(np.where(image2new!=0)).T
49 val2=image2[np.where(image2new!=0)]*1.0
50
51 dist12=cdist(loc1, loc2) #distance between all the locations
52 val=np.dot(np.array([val1]).T,np.array([val2])) #values of intensity product in these locations
53 distances=np.ravel(dist12*dxy) #putting all distances in a linear array
54 values=np.ravel(val) #putting the corresponding intensity product in a linear array
55
56 lengthscale=15
57 binwidth=0.4
58 rMax=14
59
60 Sx=Xmax-Xmin #Width of the image
61 Sy=Ymax-Ymin #Height of the image
62 XY=(Sx*Sy) #Area of the image
63 Num=np.sum(val1)*np.sum(val2)# Values of all intensity product
64 CC=np.array([0,0])
65 for dd in range(0,int(rMax/binwidth)):#preparing histogram
66     pair_hist=np.sum(values[np.where((distances>=dd*binwidth) & (distances<dd*binwidth+binwidth))])/Num
67     rand_hist=3.14*binwidth*(2*dd*binwidth+binwidth)/XY
68     CC=np.vstack([CC,[(dd+0.5)*binwidth*lengthscale,pair_hist/rand_hist]])
69
70 np.savetxt('PCC.dat', PCC,fmt='%2.2f %2.4f')

```

- [1] L Stirling Churchman, Zeynep Ökten, Ronald S Rock, John F Dawson, and James A Spudich. Single molecule high-resolution colocalization of cy3 and cy5 attached to macromolecules measures intramolecular distances through time. *Proceedings of the National Academy of Sciences*, 102(5):1419–1423, 2005.
- [2] Stefan Niekamp, Jongmin Sung, Walter Huynh, Gira Bhabha, Ronald D Vale, and Nico Stuurman. Nanometer-accuracy distance measurements between fluorophores at the single-molecule level. *Proceedings of the National*

- Academy of Sciences*, 116(10):4275–4284, 2019.
- [3] Leiting Pan, Rui Yan, Wan Li, and Ke Xu. Super-resolution microscopy reveals the native ultrastructure of the erythrocyte cytoskeleton. *Cell reports*, 22(5):1151–1158, 2018.
 - [4] Joerg Schnitzbauer, Yina Wang, Shijie Zhao, Matthew Bakalar, Tulip Nuwal, Baohui Chen, and Bo Huang. Correlation analysis framework for localization-based superresolution microscopy. *Proceedings of the National Academy of Sciences*, 115(13):3219–3224, 2018.
 - [5] Prabuddha Sengupta, Tijana Jovanovic-Talisman, Dunja Skoko, Malte Renz, Sarah L Veatch, and Jennifer Lippincott-Schwartz. Probing protein heterogeneity in the plasma membrane using palm and pair correlation analysis. *Nature methods*, 8(11):969, 2011.
 - [6] Matthew B Stone and Sarah L Veatch. Steady-state cross-correlations for live two-colour super-resolution localization data sets. *Nature communications*, 6:7347, 2015.